Scalable Fabrication of Edge Contacts to 2D Materials: Implications for Quantum Resistance Metrology and 2D Electronics

ACS APPLIED NANO MATERIALS

www.acsanm.org Article

Scalable Fabrication of Edge Contacts to 2D Materials: Implications for Quantum Resistance Metrology and 2D Electronics

Naveen Shetty, Hans He, Richa Mitra, Johanna Huhtasaari, Konstantina Iordanidou, Julia Wiktor, Sergey Kubatkin, Saroj P. Dash, Rositsa Yakimova, Lunjie Zeng, Eva Olsson, and Samuel Lara-Avila*

Cite This: *ACS Appl. Nano Mater.* 2023, 6, 6292–6298 Read Online

ACCESS | Metrics & More | Article Recommendations | Supporting Information

ABSTRACT: We report a reliable and scalable fabrication method for producing electrical contacts to two-dimensional (2D) materials based on the tri-layer resist system. We demonstrate the applicability of this method in devices fabricated on epitaxial graphene on silicon carbide (epigraphene) used as a scalable 2D material platform. For epigraphene, data on nearly 70 contacts result in median values of the one-dimensional (1D) specific contact resistances $\rho_c \sim 67\ \Omega{\cdot}\mu m$ and follow the Landauer quantum limit $\rho_c \sim n^{-1/2}$, consistently reaching values $\rho_c < 50\ \Omega{\cdot}\mu m$ at high carrier density$n$. As a proof of concept, we apply the same fabrication method to the transition metal dichalcogenide (TMDC) molybdenum disulfide (MoS_2). Our edge contacts enable MoS_2 field-effect transistor (FET) behavior with an ON/OFF ratio of $>10^6$ at room temperature ($>10^9$ at cryogenic temperatures). The fabrication route demonstrated here allows for contact metallization using thermal evaporation and also by sputtering, giving an additional flexibility when designing electrical interfaces, which is key in practical devices and when exploring the electrical properties of emerging materials.

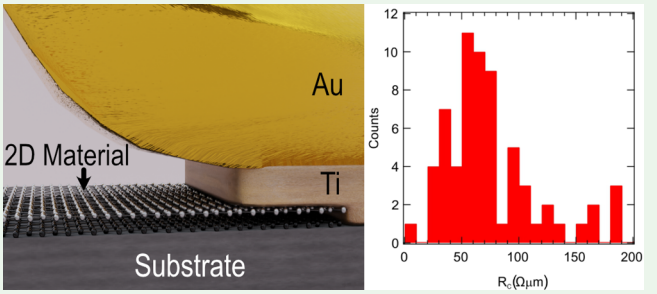

KEYWORDS: *edge-contacts, 2D material, MoS_2, graphene, epitaxial graphene*

INTRODUCTION

Two dimensional (2D) materials stand as one of the most interesting technological platforms for the development of novel and disruptive electronics.[1−3] Being atomically thin, the electron transport properties of 2D materials are extremely responsive to externally applied stimuli (e.g., light, electric field, magnetic field), making them ideal candidates for implementation of transducers with unprecedented sensitivity. Additionally, the high mobility demonstrated in some 2D materials, notably graphene, allow for devices operating at very high frequencies that are not attainable in a straightforward manner with bulk materials. Yet, a notable and often overlooked development required for the widespread use of future electronics based on 2D materials is to improve the quality, reproducibility, and reliability of the electrical contacts.[4−7] In practice, electrical interfaces to any electronic device should satisfy the following requirements: (a) allow supplying the necessary current to a device, (b) the voltage drop across the contacts should be small compared to the voltage drop across the active device region, and (c) should be stable over time and in different environments. To this day, there are some examples of successful strategies to form electrical contacts to 2D materials. However, the choice of contact materials for a particular 2D material remains somewhat of an art,[8−11] and a truly scalable fabrication of reproducible contacts to a wide variety of 2D materials remains to be demonstrated.

First proposed for carbon nanotubes, edge contacts (a.k.a. end-contacts)[12−17] are currently one of the most successful and popular methods to achieve good electrical interfacing to 2D materials. In the most common implementation of this method, originally demonstrated by the Columbia group for graphene,[15] the 2D layer is encapsulated by hexagonal boron nitride (hBN). The entire stack is then patterned and etched to expose only the edge of the graphene layer, which is subsequently metalized, to form a 1D electrical contact along the edge of graphene with 1D specific contact resistances as low as $\rho_c = 150\ \Omega{\cdot}\mu m$[15,16,18−20] in simple geometries.

Inspired by the method of forming edge contacts to graphene/hBN heterostructures, here we report a micro-fabrication strategy for the scalable microfabrication of electrical contacts to 2D materials based on the tri-layer resist system,[21] which does not require encapsulation of the 2D material by hBN. Recently, we have used this method to

Received: February 11, 2023
Accepted: March 20, 2023
Published: March 30, 2023

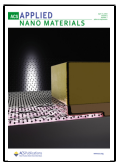

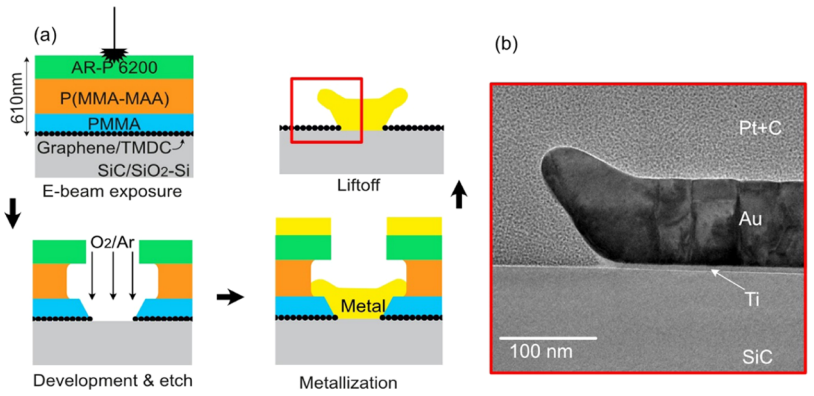

Figure 1. Formation of scalable edge contacts to 2D materials. (a) Schematic representation of the tri-layer resist method for fabrication of edge contacts to 2D materials. (b) Transmission electron microscopy (TEM) image of the edge-contact formation between graphene and Ti/Au contact.

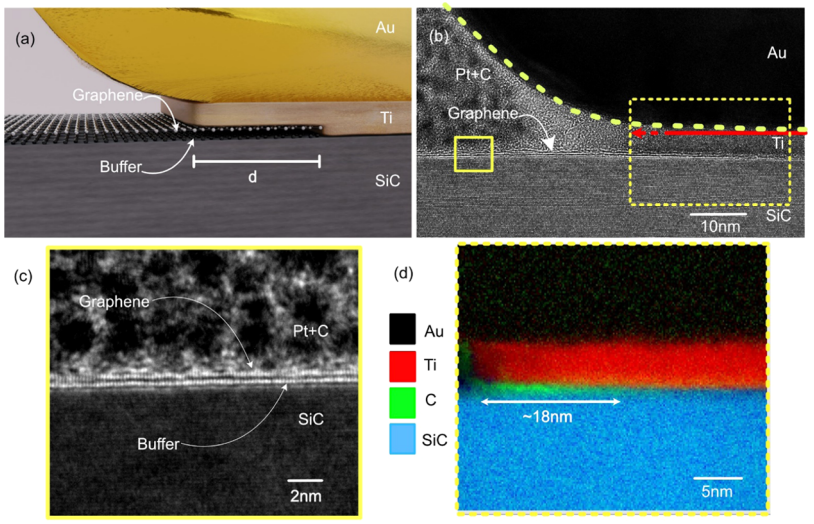

Figure 2. TEM analysis of contacts to epigraphene. (a) Illustration of the graphene and buffer layer in contact with Ti/Au contact. (b) TEM image showing epigraphene–metal contact. The Pt + C layer is a protection layer deposited during TEM sample preparation. (c) TEM image of the area enclosed by the yellow rectangle in panel (b), showing the presence of epitaxial graphene and buffer over SiC. (d) STEM-EELS chemical mapping of the interface between graphene and metal contacts. The chemical analysis reveals that epigraphene is contacted at the edge and that Ti covers the graphene top surface over a distance $d \sim 18$ nm.

produce nearly 3000 contacts to graphene and demonstrated the largest, most accurate array of graphene quantum resistors,[22] using epitaxial graphene on silicon carbide (epigraphene).[23] This demanding application requires 100 % yield, i.e., the total contribution of all contact resistances has to be well below 100 nanoOhms. To demonstrate the versatility of the edge-contact fabrication method, we expand its use to another 2D material platform, the transition metal dichalcogenide (TMDC) molybdenum disulfide (MoS_2). Our proof-of-concept tests utilizing the edge-contact fabrication process on TMDCs yield robust and reproducible metallization, resulting in MoS_2 flakes in a field-effect transistor (FET) configuration with linear current–voltage (I–V) characteristics and ON/OFF ratios of $>10^6$ at room temperature.

Fabrication of Edge Contacts. Figure 1a shows the principle of the edge-contact microfabrication method using the tri-layer resist system. The key to ensure scalable and reproducible contacts is to form a narrow/wide/narrow opening in the resist, which we achieve in a single e-beam exposure and single development step by using a resist with higher sensitivity (compared to the top and bottom layers) as the middle layer (see the Methods section and Supporting Information S1). After the resist development step, dry etching is used to remove the 2D material and expose its edges for a subsequent metallization step and metal liftoff. Figure 1b shows a transmission electron microscopy (TEM) image that exemplifies the contact geometry achieved for the case of epigraphene and SiC, where dry etching is performed with oxygen plasma. By using the tri-layer resist method, compared to, e.g., single layer method,[24] we have observed a remarkably high yield in the fabrication of contacts and reproducibility in achieving consistently low contact resistance demonstrated in this and in our earlier work.[22] This is because the resist profile provides a clean liftoff when the metal deposition is performed by thermal evaporation and also by sputtering, thus giving additional flexibility when designing a microfabrication process.

Figure 2a shows an illustration of the edge-contact formation between epigraphene and Ti/Au, as revealed by TEM. For this material, our process results in a contact to graphene such that the edge of the crystal and a small portion of its top surface (d < 20 nm) are directly contacted by the metal adhesion layer

https://doi.org/10.1021/acsanm.3c00652
ACS Appl. Nano Mater. 2023, 6, 6292–6298

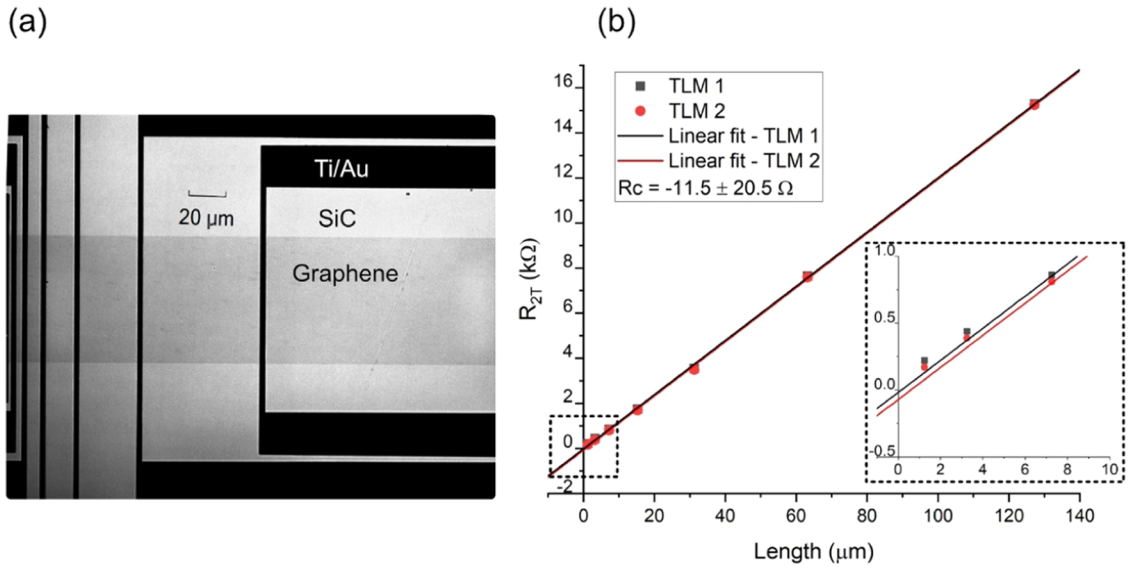

Figure 3. Characterization of contacts to epigraphene by the transfer length method (TLM). (a) Transmission mode optical microscopy image of the fabricated edge-contacted TLM device. (b) Example of TLM data for two devices with 64 μm wide epigraphene channels measured at T = 300 K. Note that the corresponding fit yields a negative (unphysical) R_c, close to zero value, with uncertainty ±20.5 Ω. Inset: zoom into the TLM data for L < 10 μm.

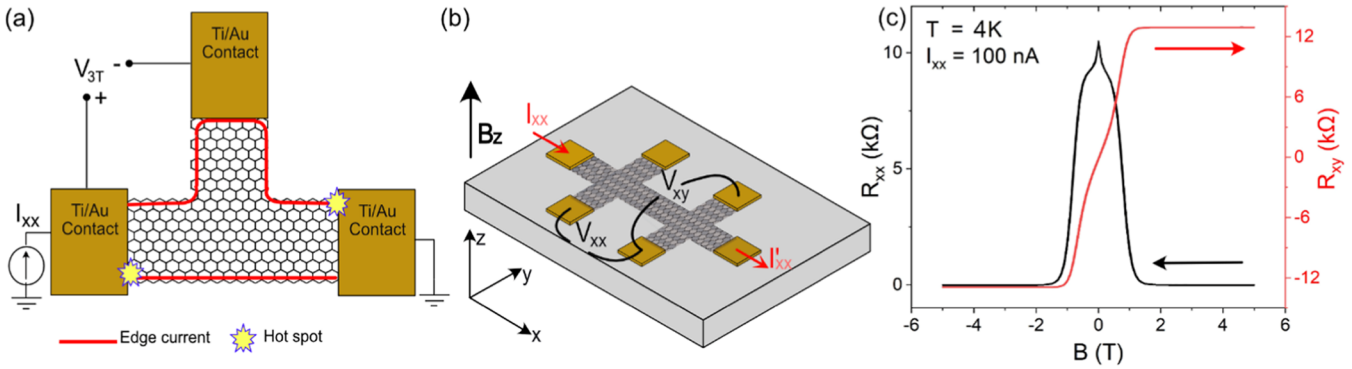

Figure 4. Illustration of three- and four-terminal resistance measurements of epigraphene in quantum Hall regime. (a) Schematic of three-terminal contact measurement on a Hall bar. In the quantum Hall regime, the channel resistance vanishes due to the formation of edge states, and the measured three-terminal resistance, $R_{3T} = V_{3T}/I_{xx}$, includes R_c and the (known) resistance of the leads $2R_m$. (b) Schematic of the measurements to extract the longitudinal resistance $R_{xx} = V_{xx}/I_{xx}$ and transverse resistance $R_{xy} = V_{xy}/I_{xx}$ measurement on a Hall bar. (c) Measured R_{xx} (black) and R_{xy} (red) in quantum Hall regime. In our devices, R_{xx} = 0 is obtained at B < 2T, and the QHE persists to temperatures up to T = 8 K and 100 nA.

(Ti). Figure 2b shows an overview TEM image of the area around the graphene–metal contact. Figure 2c is a zoomed-in TEM image of a region ∼ 30 nm away from the metallization area (yellow square in Figure 2b), showing the presence of the two carbon layers of epigraphene, i.e., buffer layer in contact with SiC and graphene as the top-most layer. The two carbon layers are atomically flat and continuously cover the whole SiC substrate, except the contact region. Regarding the details of the metal–graphene interface, we have used scanning TEM (STEM)-electron energy loss spectroscopy (EELS) to determine the boundary where graphene starts to be in contact with metal (Ti). Figure 2d is a false color map of the STEM-EELS chemical mapping at the contact edge, and it shows that graphene (green) is indeed contacted at the edge, but also part of its top surface is in contact with the titanium (red), over an extent d ∼ 18 nm. This chemical analysis establishes that the metal–graphene contact region occurs in the area approximately denoted by the dashed box in Figure 2b.

Electrical Characterization of Edge Contacts to Epigraphene. To illustrate the low contact resistance obtained using this fabrication method, we start describing the work performed on epigraphene, a wafer-scale material that allows us to fabricate large, ∼ mm-sized devices. For initial characterization, we used the standard transfer length method (TLM).[25] For this, graphene test structures of channel width W are fitted with electrical contacts that are separated by a varying distance L (Figure 3a). The measured two-terminal resistance R_{2T} between adjacent contacts is

$$R_{2T} = 2R_m + 2R_c + R_{channel} \quad (1)$$

which includes the (known) contribution of the metallic leads R_m, the metal–graphene interface R_c, and the graphene channel resistance, $R_{channel} = \rho L/W$, with ρ being the resistivity of graphene. A plot of the measured R_{2T} vs the contact spacing will be, in principle, a straight line, where the resistivity of the material can be found from the slope, $dR_{2T}/dL = \rho/W$, and the contact resistance can be extracted from the intercept at L = 0, $R_{2T}(L = 0) = 2R_m + 2R_c$.

https://doi.org/10.1021/acsanm.3c00652
ACS Appl. Nano Mater. 2023, 6, 6292–6298

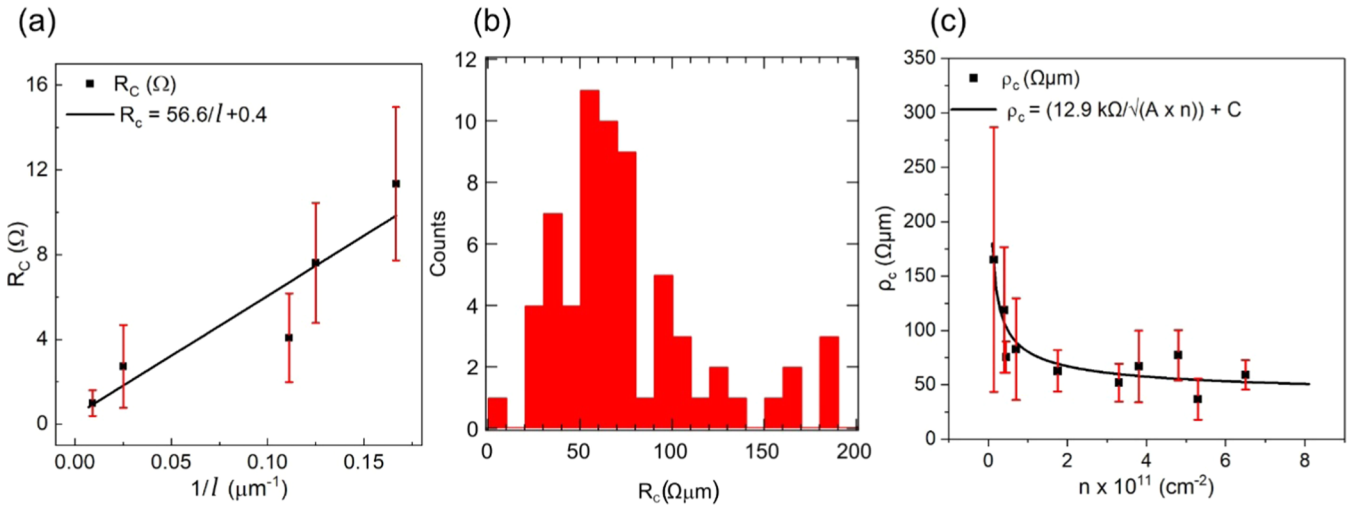

Figure 5. Metal−graphene interface characterization using the three-probe configuration in quantum hall regime (T = 4 K, B = 5 T). (a) R_c (Ω) as a function of inverse perimeter length for five devices placed on the same chip. The linear fit yields a resistance $R_c(l) = 56.6/l + 0.4$ Ω. (b) Histogram of almost 70 edge contacts for nine devices placed on three different epigraphene chips. Contacts with higher $\rho_c > 110$ Ω·μm are due to lowly doped graphene $n < 1 \times 10^{11}$ cm^{-2}. (c) ρ_c as a function of carrier concentration. The solid line is fit to $\rho_c = h/(2e^2\sqrt{n_{eff}}) + C$, with $n_{eff} = A \times n$. Here, n_{eff} is an effective carrier density at the carrier injection points (hot spots). Our fits return the values A = 19.7 and C = 34.5 Ω·μm. All error bars represent one standard deviation from the mean value.

In total, we have performed TLM measurements on 12 epigraphene structures patterned on five epigraphene chips. Prior to measurements, samples were encapsulated to control and stabilize the doping of epigraphene.[26] The graphene channel width W varied from 8−64 μm, and the distance L varied from 1−128 μm. Figure 3b shows an example of a TLM plot, R_{2T} vs L, for the two largest epigraphene devices, W = 64 μm and total length of 270 μm. In this plot, each resistance data point is extracted from a linear fit to current−voltage curves (I−V) using a voltage bias up to V = 1 mV. The first observation is that the slope of the two devices is remarkably similar, dR_{2T}/dL = 119 Ω/μm, giving a sheet resistance of 7616 Ω/□. As for the intercept, our linear fit yields a value of R_c very close to zero, with an uncertainty of ±20.5 Ω. Quantitively, this indicates that the contacts provide an electrical interface with very low contact resistance, and this is achieved for all of the fabricated TLM structures with good reproducibility. The uncertainty in the TLM measurements is relatively low, not uncommon, and it may arise from, e.g., local variations in the material doping or the geometry of the fabricated devices (See Supporting Information S2).

To accurately quantify the contact resistance of our contacts, we turn to a Hall bar geometry and exploit the possibility offered by epigraphene to characterize the transparency of metal−graphene interface using a three-probe measurement R_{3T} under quantum Hall effect conditions (QHE).[7,27] In this three-probe measurement scheme (Figure 4a), the total measured resistance is

$$R_{3T} = 2R_m + R_c + R_{channel} \quad (2)$$

At low temperatures and in quantizing magnetic field,[28] the graphene channel resistance vanishes, $R_{channel} = 0$, and a three-terminal measurement gives a direct measurement of the metal−graphene interface resistance R_c. Figure 4b,c shows the configuration and outcome, respectively, of the quantum Hall characterization of devices performed prior to measurement of contact resistance to ensure that the channel resistance $R_{channel} = V_{xx}/I_{xx} = 0$, and the transversal resistivity ($R_{xy} = V_{xy}/I_{xx}$) acquires the quantized value of $R_{xy} = h/2e^2 \approx 12.9$ kΩ, where h is the Plank constant and e is the elementary charge.

Figure 5a shows that the typical phenomenology of our metal−graphene interface is that of edge contacts, i.e., the linear dependence of R_c (Ω) on the inverse contact perimeter $1/l$. Furthermore, this behavior in fact extends to graphene in QHE.[15,29] These measurements were performed on five devices placed on the same chip, where the carrier density is tuned to $n \approx 10^{10}$−10^{11} cm^{-2}. For comparison among devices placed on different chips (nine devices in three different epigraphene chips), we calculate and present the 1D specific contact resistance $\rho_c = R_c \times l$, with l being the perimeter length. Figure 5b shows a histogram of ρ_c obtained for nearly 70 Ti/Au edge contacts to epigraphene, with a mean value of $\bar{\rho}_c$ = 82 Ω·μm and a median value at $\tilde{\rho}_c$ = 67 Ω·μm. These statistics indicate that our tri-layer resist method can reproducibly produce contacts with low contact resistance. The spread in contact resistance values arises from the different doping of epigraphene in different chips. This is shown in Figure 5c, which displays the specific contact resistance data as a function of the carrier density n measured in the devices from the low-field magnetoresistance data $n = 1/eR_H$, with the Hall coefficient $R_H = dR_{xy}/dB$, and e the elementary charge. The specific contact resistance follows the functional form for the Landauer quantum limit of resistance,[5] $\rho_c^{min} = h/(2e^2k_F) \approx 12\,906.403/\sqrt{n_{2D}}$ Ω·μm. As the charge density is reduced below 1×10^{11} cm^{-2}, the larger error bars in our measurements can be attributed to the larger effect of (local) charge inhomogeneity at the graphene−metal interface (charge puddles).[30,31] As a note, the R_c measured in three-probe geometry in QHE arises from the region where current injection takes place, the so-called "hotspot," where all of the dissipation and voltage drop takes place (see Figure 4a).[32,33] From the $\propto l^{-1}$ and $\propto n^{-1/2}$ dependence of contact resistance, it appears that at the hotspot regions, electron transfer at the interface between metal and graphene in a high magnetic field (i.e., in QHE) keeps similarities with electron injection into graphene at B = 0. The main difference we observe around this

https://doi.org/10.1021/acsanm.3c00652
ACS Appl. Nano Mater. 2023, 6, 6292−6298

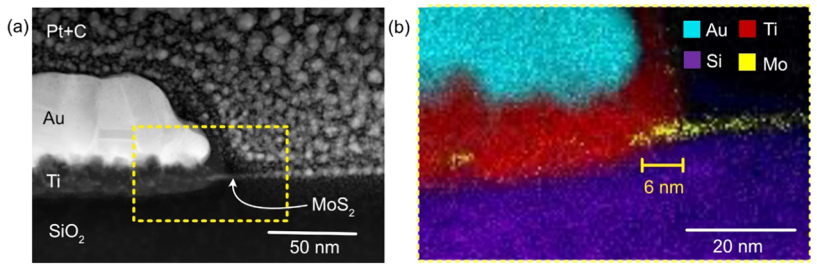

Figure 6. TEM analysis of contacts to MoS_2. (a) Annular dark-field (ADF) scanning TEM (STEM) image of the edge contact between MoS_2 and Ti/Au (5/55 nm). (b) STEM-XEDS composition map of the interface between MoS_2 and metal contacts.

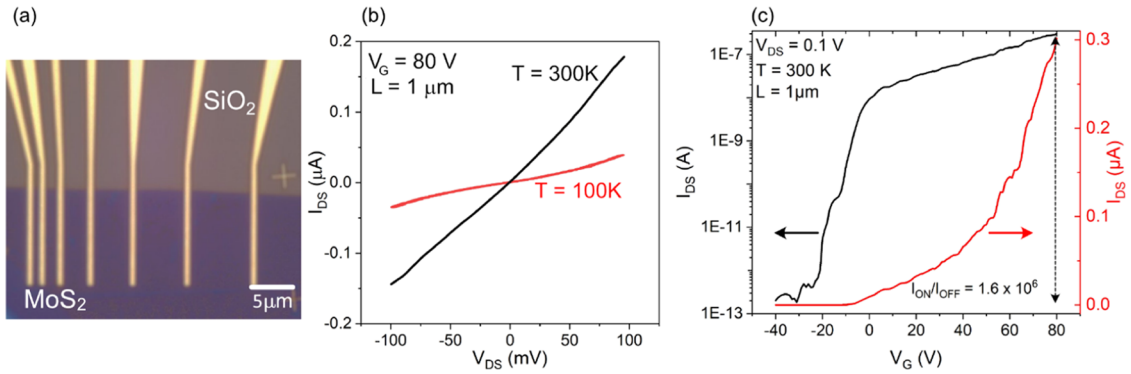

Figure 7. Contacts to molybdenum disulfide (MoS_2). (a) Optical microscope image of the fabricated MoS_2 FET device. (b) (I–V) measured in the ON state (gate voltage V_G = 80 V) at room temperature and T = 100 K. (c) Transfer characteristic of the MoS_2 device for V_{DS} = 0.1 V, T = 300 K.

region is an effective carrier density about an order of magnitude higher than that extracted from the low field.

Edge Contacts for Transition Metal Dichalcogenides. Having demonstrated the low contact resistance reproducibly achieved for epigraphene, we show that the fabrication process (Figure 1a) can be readily applicable to a wider class of 2D materials, using semiconducting MoS_2 as an example. A notable difference from contacting epigraphene is that for this material, we avoid the oxygen plasma step, and the best results are obtained by in situ ion milling before metal deposition. Moreover, after the metallization and liftoff steps, and prior to electrical measurements, samples are annealed at 180 °C in 3 × 10^{-6} mbar vacuum (see the Methods section). Figure 6a shows an annular dark-field (ADF) STEM image of the MoS_2/Ti interface, and Figure 6b shows the corresponding elemental distribution in the same area obtained using STEM-X-ray energy dispersive spectroscopy (XEDS). This analysis reveals that, as in the case of epigraphene, the 2D material is contacted at the edge and the top surface over a distance of about d = 6 nm. This confirms the robustness of the contact fabrication process, which can successfully contact the material edge irrespective of the growth/transfer process, type of metallization, and type of substrate used.

The electrical test of the contacts formed to MoS_2 is shown in Figure 7. Figure 7a shows a device prepared using a few-layer MoS_2 flake (about three layers, thickness 2.5 nm) as the channel material. Ti (10 nm)/Au (50 nm) has been evaporated to form contact spacing over lengths L = 1, 2, 3, and 4 μm, limited by the size of the flakes (2.5–10 μm^2).

Figure 7b shows the I–V characteristic of the MoS_2 device across the shortest contact separation, L = 1 μm, in the ON state (V_G = 80 V) for temperatures T = 100 K and 300 K. (See Supporting Information S3 for other channels lengths). The linearity of the I–V curves for all contact spacings indicates that the achieved contacts are ohmic. Figure 7c shows the field-effect transfer characteristic of the device at room temperature, with an ON/OFF ratio of $I_{on}/I_{off} > 10^6$ ($I_{on}/I_{off} > 10^7$ at high bias, $I_{on}/I_{off} \approx 10^{10}$ at low temperatures, see Supporting Information S4). These values match with the state-of-the-art ON/OFF ratios of TMDC field-effect devices reported,[8,34] suggesting that the high-quality electrical interface achieved with our contact method could be promising to push the limits of TMDC devices.

CONCLUSIONS

We foresee that the method to form edge contacts for epigraphene and MoS_2 can be readily applicable to a wide variety of materials, including bulk and low-dimensional materials. Here, we have demonstrated using e-beam lithography that the narrow/wide/narrow opening in resist can lead to scalable fabrication of edge contacts to 2D materials. It is possible that the same results can also be achieved by optical lithography methods with some effort and careful choice of resist layers. The process can be further optimized to achieve a different contact profile by fine-tuning the lithography parameters (e.g., a different combination of resist, solvents, and irradiation dose, see also Supporting Information Figure S1). The possibility to avoid encapsulation of the 2D material channel by, e.g., hBN to form edge contacts could be especially suitable for chemical or gas sensors, where the channel material must be exposed to chemical analytes to achieve transduction. More generally, good electrical interfaces are key to achieving low noise performance in practical electronic devices. The possibility to achieve metal deposition by thermal evaporation and also by sputtering gives an additional advantage when designing electrical interfaces, which is key in exploring the electrical properties of emerging materials.

https://doi.org/10.1021/acsanm.3c00652
ACS Appl. Nano Mater. 2023, 6, 6292–6298

METHODS

Materials. MoS_2 flakes were exfoliated and transferred onto Si−SiO_2 substrates using the scotch tape technique and poly(dimethylsiloxane) (PDMS) dry transfer. The SiO_2 substrate is about 300 nm thick. The typical thickness of a prepared flake is 2 ± 0.5 nm. Epigraphene was grown on 4H−SiC chips (7 × 7 mm^2), which were encased in a graphite crucible and heated by RF heating to around 1850 °C in an inert argon atmosphere of 1 bar.

Devices. For contact formation, we deposit a tri-layer of commercially available electron beam sensitive resists: 150 nm thick PMMA, 280 nm thick P(MMA-MAA) copolymer, and 180 nm thick AR-P 6200.13 (see Figure 1a). After e-beam patterning, the topmost layer (AR-P 6200.13) is developed using *o*-xylene. For the bottom resist layers, we exploit the different sensitivities of PMMA and P(MMA-MAA) to the same developer, 93% IPA and 7% H_2O. This ensures the desired undercut that facilitates liftoff. After the development is completed, epitaxial graphene chips are etched by 1 min of O_2-plasma at 50 W and 250 mT. For MoS_2 chips, in situ Ar-plasma etching (1 min) is performed before metal deposition. This step is achieved in a Lesker PVD225 deposition system equipped with an end-Hall linear ion source operating at 170 V, 2 Amps, and 2.2 × 10^{-4} Torr. Metal deposition (Ti 5 nm and Au 100 nm) is performed at pressure $P = 5 \times 10^{-7}$ mbar. A second lithography step and O_2-plasma are used for graphene to define the geometry of devices.

To avoid the ears at the edge of metal contacts as seen in Figure 1a, the resist thickness is adjusted to 70 nm thick PMMA, 80 nm thick P(MMA-MAA) copolymer, and 70 nm thick AR-P 6200.13. The thickness of the metal in this case reduced to 5 nm Ti and 55 nm Au.

Electrical Measurements. Standard electrical characterization was performed in a liquid 4He gas flow cryostat, which allowed for temperatures down to 2 K and magnetic fields up to 14 T. All reported values of charge carrier mobility and charge carrier concentration were extracted from four-probe Hall and quantum Hall measurements. The standard measurement setup used current biased samples at a maximum of 100 nA DC (Keithley 6221 DC and AC current source, Agilent 34420 A nanovoltmeter).

Transmission Electron Microscopy. TEM lamellas of the contacts were prepared using an FEI Versa focused ion beam−scanning electron microscope (FIB−SEM). Final polishing of the lamellas in FIB−SEM was performed with an ion beam energy of 2 kV and beam current of ∼ 20 pA to minimize beam effect. For TEM analysis, a JEOL monochromated ARM200F TEM was operated at 200 kV. The TEM is equipped with a CEOS GmbH probe corrector, a double silicon drift detector (SSD) for X-ray energy dispersive spectroscopy (XEDS), and Gatan GIF Continuum for electron energy loss spectroscopy (EELS). STEM-EELS and STEM−XEDS spectrum imaging measurements are used for elemental mapping.

ASSOCIATED CONTENT

Supporting Information

The Supporting Information is available free of charge at https://pubs.acs.org/doi/10.1021/acsanm.3c00652.

> Additional experimental details and methods; comparison of microfabrication of edge contacts using one or two electron beam lithography (EBL) steps, and current−voltage characteristics of MoS_2 devices (PDF)

AUTHOR INFORMATION

Corresponding Author

Samuel Lara-Avila − *Department of Microtechnology and Nanoscience, Chalmers University of Technology, 412 96 Gothenburg, Sweden; National Physical Laboratory, Middlesex TW11 0LW, U.K.;* orcid.org/0000-0002-8331-718X; Email: samuel.lara@chalmers.se

Authors

Naveen Shetty − *Department of Microtechnology and Nanoscience, Chalmers University of Technology, 412 96 Gothenburg, Sweden;* orcid.org/0000-0002-1230-7048

Hans He − *Department of Microtechnology and Nanoscience, Chalmers University of Technology, 412 96 Gothenburg, Sweden; RISE Research Institutes of Sweden, S-50115 Borås, Sweden;* orcid.org/0000-0003-1962-5572

Richa Mitra − *Department of Microtechnology and Nanoscience, Chalmers University of Technology, 412 96 Gothenburg, Sweden;* orcid.org/0000-0001-8852-6645

Johanna Huhtasaari − *Department of Microtechnology and Nanoscience, Chalmers University of Technology, 412 96 Gothenburg, Sweden;* orcid.org/0000-0003-1653-9476

Konstantina Iordanidou − *Department of Physics, Chalmers University of Technology, 412 96 Gothenburg, Sweden;* orcid.org/0000-0003-4696-8204

Julia Wiktor − *Department of Physics, Chalmers University of Technology, 412 96 Gothenburg, Sweden;* orcid.org/0000-0003-3395-1104

Sergey Kubatkin − *Department of Microtechnology and Nanoscience, Chalmers University of Technology, 412 96 Gothenburg, Sweden;* orcid.org/0000-0001-8551-9247

Saroj P. Dash − *Department of Microtechnology and Nanoscience, Chalmers University of Technology, 412 96 Gothenburg, Sweden;* orcid.org/0000-0001-7931-4843

Rositsa Yakimova − *Department of Physics, Chemistry and Biology, Linköping University, 581 83 Linköping, Sweden;* orcid.org/0000-0003-4237-2702

Lunjie Zeng − *Department of Physics, Chalmers University of Technology, 412 96 Gothenburg, Sweden;* orcid.org/0000-0002-4564-7217

Eva Olsson − *Department of Physics, Chalmers University of Technology, 412 96 Gothenburg, Sweden;* orcid.org/0000-0002-3791-9569

Complete contact information is available at: https://pubs.acs.org/10.1021/acsanm.3c00652

Author Contributions

The manuscript was written through contributions of all authors. All authors have given approval to the final version of the manuscript.

Funding

This work was jointly supported by the Swedish Foundation for Strategic Research (SSF) (Nos. GMT14-0077, RMA15-0024, and FFL21-0129), Chalmers Area of Advance Nano, Chalmers Area of Advance Energy, 2D TECH VINNOVA competence Center (Ref. 2019-00068), Marie Sklodowska-Curie grant QUESTech No. 766025, Knut and Alice Wallenberg Foundation (2019.0140), and the Swedish Research Council VR (Contract Nos. 2021-05252 and 2018-04962). This work was performed in part at Myfab Chalmers and Chalmers Materials Analysis Laboratory (CMAL). The authors declare that the main data supporting the findings of this study are available within the article and supplementary information. Additional data are available from the corresponding author upon request.

Notes

The authors declare no competing financial interest.

REFERENCES

(1) Fiori, G.; Bonaccorso, F.; Iannaccone, G.; Palacios, T.; Neumaier, D.; Seabaugh, A.; Banerjee, S. K.; Colombo, L. Electronics Based on Two-Dimensional Materials. *Nat. Nanotechnol.* **2014**, *9*, 768−779.

(2) Zeng, S.; Tang, Z.; Liu, C.; Zhou, P. Electronics Based on Two-Dimensional Materials: Status and Outlook. *Nano Res.* **2021**, *14*, 1752−1767.

(3) Akinwande, D.; Huyghebaert, C.; Wang, C. H.; Serna, M. I.; Goossens, S.; Li, L. J.; Wong, H. S. P.; Koppens, F. H. L. Graphene and Two-Dimensional Materials for Silicon Technology. *Nature* **2019**, *573*, 507−518.

(4) Parrish, K. N.; Akinwande, D. Impact of Contact Resistance on the Transconductance and Linearity of Graphene Transistors. *Appl. Phys. Lett.* **2011**, *98*, No. 183505.

(5) Allain, A.; Kang, J.; Banerjee, K.; Kis, A. Electrical Contacts to Two-Dimensional Semiconductors. *Nat. Mater.* **2015**, *14*, 1195−1205.

(6) Xia, F.; Perebeinos, V.; Lin, Y. M.; Wu, Y.; Avouris, P. The Origins and Limits of Metal-Graphene Junction Resistance. *Nat. Nanotechnol.* **2011**, *6*, 179−184.

(7) Yager, T.; Lartsev, A.; Cedergren, K.; Yakimova, R.; Panchal, V.; Kazakova, O.; Tzalenchuk, A.; Kim, K. H.; Park, Y. W.; Lara-Avila, S.; Kubatkin, S. Low Contact Resistance in Epitaxial Graphene Devices for Quantum Metrology. *AIP Adv.* **2015**, *5*, No. 087134.

(8) Shen, P. C.; Su, C.; Lin, Y.; Chou, A. S.; Cheng, C. C.; Park, J. H.; Chiu, M. H.; Lu, A. Y.; Tang, H. L.; Tavakoli, M. M.; Pitner, G.; Ji, X.; Cai, Z.; Mao, N.; Wang, J.; Tung, V.; Li, J.; Bokor, J.; Zettl, A.; Wu, C. I.; Palacios, T.; Li, L. J.; Kong, J. Ultralow Contact Resistance between Semimetal and Monolayer Semiconductors. *Nature* **2021**, *593*, 211−217.

(9) Moon, J. S.; Antcliffe, M.; Seo, H. C.; Curtis, D.; Lin, S.; Schmitz, A.; Milosavljevic, I.; Kiselev, A. A.; Ross, R. S.; Gaskill, D. K.; Campbell, P. M.; Fitch, R. C.; Lee, K. M.; Asbeck, P. Ultra-Low Resistance Ohmic Contacts in Graphene Field Effect Transistors. *Appl. Phys. Lett.* **2012**, *100*, No. 203512.

(10) Robinson, J. A.; LaBella, M.; Zhu, M.; Hollander, M.; Kasarda, R.; Hughes, Z.; Trumbull, K.; Cavalero, R.; Snyder, D. Contacting Graphene. *Appl. Phys. Lett.* **2011**, *98*, No. 053103.

(11) Tzalenchuk, A.; Lara-Avila, S.; Cedergren, K.; Syväjärvi, M.; Yakimova, R.; Kazakova, O.; Janssen, T. J. B. M.; Moth-Poulsen, K.; Bjørnholm, T.; Kopylov, S.; Fal, V.; Kubatkin, S. Engineering and Metrology of Epitaxial Graphene. *Solid State Commun.* **2011**, *151*, 1094−1099.

(12) Tersoff, J. Contact Resistance of Carbon Nanotubes. *Appl. Phys. Lett.* **1999**, *74*, 2122−2124.

(13) Matsuda, Y.; Deng, W. Q.; Goddard, W. A. Contact Resistance Properties between Nanotubes and Various Metals from Quantum Mechanics. *J. Phys. Chem. C* **2007**, *111*, 11113−11116.

(14) Matsuda, Y.; Deng, W. Q.; Goddard, W. A. Contact Resistance for "End-Contacted" Metal-Graphene and Metal-Nanotube Interfaces from Quantum Mechanics. *J. Phys. Chem. C* **2010**, *114*, 17845−17850.

(15) Wang, L.; Meric, I.; Huang, P. Y.; Gao, Q.; Gao, Y.; Tran, H.; Taniguchi, T.; Watanabe, K.; Campos, L. M.; Muller, D. A.; Guo, J.; Kim, P.; Hone, J.; Shepard, K. L.; Dean, C. R. One-Dimensional Electrical Contact to a Two-Dimensional Material. *Science* **2013**, *342*, 614−617.

(16) Choi, M. S.; Ali, N.; Ngo, T. D.; Choi, H.; Oh, B.; Yang, H.; Yoo, W. J. Recent Progress in 1D Contacts for 2D-Material-Based Devices. *Adv. Mater.* **2022**, *34*, No. 2202408.

(17) Parto, K.; Pal, A.; Chavan, T.; Agashiwala, K.; Yeh, C. H.; Cao, W.; Banerjee, K. One-Dimensional Edge Contacts to Two-Dimensional Transition-Metal Dichalcogenides: Uncovering the Role of Schottky-Barrier Anisotropy in Charge Transport across Mo S2 /Metal Interfaces. *Phys. Rev. Appl.* **2021**, *15*, No. 064068.

(18) Xiao, J.; Kang, Z.; Liu, B.; Zhang, X.; Du, J.; Chen, K.; Yu, H.; Liao, Q.; Zhang, Z.; Zhang, Y. Record-High Saturation Current in End-Bond Contacted Monolayer MoS2 Transistors. *Nano Res.* **2022**, *15*, 475−481.

(19) Blake, P.; Yang, R.; Morozov, S. V.; Schedin, F.; Ponomarenko, L. A.; Zhukov, A. A.; Nair, R. R.; Grigorieva, I. V.; Novoselov, K. S.; Geim, A. K. Influence of Metal Contacts and Charge Inhomogeneity on Transport Properties of Graphene near the Neutrality Point. *Solid State Commun.* **2009**, *149*, 1068−1071.

(20) Aslanidou, S.; García-García, A.; Godignon, P.; Rius, G. Electronic Interface and Charge Carrier Density in Epitaxial Graphene on Silicon Carbide. A Review on Metal-Graphene Contacts and Electrical Gating. *APL Mater.* **2020**, *8*, No. 100702.

(21) Lai, Y.-L.; Chang, E. Y.; Chang, C. Y.; Yang, H. P. D.; Nakamura, K.; Shy, S. L. A Simple Fabrication Process of T-Shaped Gates Using a Deep-UV/Electron-Beam/Deep-UV Tri-Layer Resist System and Electron-Beam Lithography. *Jpn. J. Appl. Phys.* **1996**, *35*, No. 6440.

(22) He, H.; Cedergren, K.; Shetty, N.; Lara-Avila, S.; Kubatkin, S.; Bergsten, T.; Eklund, G. Accurate Graphene Quantum Hall Arrays for the New International System of Units. *Nat. Commun.* **2022**, *13*, No. 6933.

(23) Virojanadara, C.; Syväjarvi, M.; Yakimova, R.; Johansson, L.; Zakharov, a.; Balasubramanian, T. Homogeneous Large-Area Graphene Layer Growth on 6H-SiC(0001). *Phys. Rev. B* **2008**, *78*, No. 245403.

(24) Cheng, Z.; Yu, Y.; Singh, S.; Price, K.; Noyce, S. G.; Lin, Y. C.; Cao, L.; Franklin, A. D. Immunity to Contact Scaling in MoS2 Transistors Using in Situ Edge Contacts. *Nano Lett.* **2019**, *19*, 5077−5085.

(25) Shockley, W.; Goetzberger, A.; Scarlett, R. M.; Finch, R.; Gereth, R.; Williams, V.; Zetterquist, N. *Research and Investigation of Inverse Epitaxial UHF Power Transistors*, Report. No Al-TOR-64-207, 1964.

(26) He, H.; Kim, K. H.; Danilov, A.; Montemurro, D.; Yu, L.; Park, Y. W.; Lombardi, F.; Bauch, T.; Moth-Poulsen, K.; Iakimov, T.; Yakimova, R.; Malmberg, P.; Müller, C.; Kubatkin, S.; Lara-Avila, S. Uniform Doping of Graphene Close to the Dirac Point by Polymer-Assisted Assembly of Molecular Dopants. *Nat. Commun.* **2018**, *9*, No. 3956.

(27) Delahaye, F. Technical Guidelines for Reliable Measurements of the Quantized Hall Resistance. *Metrologia* **1989**, *26*, 63−68.

(28) Klitzing, K. V.; Dorda, G.; Pepper, M. New Method for High-Accuracy Determination of the Fine-Structure Constant Based on Quantized Hall Resistance. *Phys. Rev. Lett.* **1980**, *45*, 494−497.

(29) Nagashio, K.; Nishimura, T.; Kita, K.; Toriumi, A. Contact Resistivity and Current Flow Path at Metal/Graphene Contact. *Appl. Phys. Lett.* **2010**, *97*, No. 143514.

(30) Zhang, Y.; Brar, V. W.; Girit, C.; Zettl, A.; Crommie, M. F. Origin of Spatial Charge Inhomogeneity in Graphene. *Nat. Phys.* **2009**, *5*, 722−726.

(31) Martin, J.; Akerman, N.; Ulbricht, G.; Lohmann, T.; Smet, J. H.; Von Klitzing, K.; Yacoby, A. Observation of Electron-Hole Puddles in Graphene Using a Scanning Single-Electron Transistor. *Nat. Phys.* **2008**, *4*, 144−148.

(32) Wakabayashi, J.-i.; Kawaji, S. Hall Effect in Silicon MOS Inversion Layers under Strong Magnetic Fields. *J. Phys. Soc. Jpn.* **1978**, *44*, 1839−1849.

(33) Meziani, Y. M.; Chaubet, C.; Bonifacie, S.; Raymond, A.; Poirier, W.; Piquemal, F. Behavior of the Contacts of Quantum Hall Effect Devices at High Currents. *J. Appl. Phys.* **2004**, *96*, 404−410.

(34) Nourbakhsh, A.; Zubair, A.; Sajjad, R. N.; Amir, T. K. G.; Chen, W.; Fang, S.; Ling, X.; Kong, J.; Dresselhaus, M. S.; Kaxiras, E.; Berggren, K. K.; Antoniadis, D.; Palacios, T. MoS2 Field-Effect Transistor with Sub-10 Nm Channel Length. *Nano Lett.* **2016**, *16*, 7798−7806.

https://doi.org/10.1021/acsanm.3c00652
ACS Appl. Nano Mater. 2023, 6, 6292−6298